remote sensing

MDPI

Article

A Five-Component Decomposition Method with General Rotated Dihedral Scattering Model and Cross-Pol Power Assignment

Yancui Duan [1], Sinong Quan [1,*], Hui Fan [2], Zhenhai Xu [1] and Shunping Xiao [1]

[1] State Key Laboratory of Complex Electromagnetic Environment Effects on Electronics and Information System, National University of Defense Technology, Changsha 410073, China; duanyancui@nudt.edu.cn (Y.D.); drxzh930@sina.com (Z.X.); xiaoshunping@nudt.edu.cn (S.X.)

[2] College of Computer Science and Information Technology, Central South University of Forestry and Technology, Changsha 410004, China; t20142226@csuft.edu.cn

* Correspondence: quansinong13@nudt.edu.cn; Tel.: +86-132-9865-7814

Abstract: The model-based polarimetric decomposition is extensively studied due to its simplicity and clear physical interpretation of Polarimetric Synthetic Aperture Radar (PolSAR) data. Though there are many fine basic scattering models and well-designed decomposition methods, the overestimation of volume scattering (OVS) may still occur in highly oriented buildings, resulting in severe scattering mechanism ambiguity. It is well known that not only vegetation areas but also oriented buildings may cause intense cross-pol power. To improve the scattering mechanism ambiguity, an appropriate scattering model for oriented buildings and a feasible strategy to assign the cross-pol power between vegetation and oriented buildings are of equal importance. From this point of view, we propose a five-component decomposition method with a general rotated dihedral scattering model and an assignment strategy of cross-pol power. The general rotated dihedral scattering model is established to characterize the integral and internal cross-pol scattering from oriented buildings, while the assignment of cross-pol power between volume and rotated dihedral scattering is achieved by using an eigenvalue-based descriptor D_{OOB}. In addition, a simple branch condition with explicit physical meaning is proposed for model parameters inversion. Experiments on spaceborne Radarsat−2 C band and airborne UAVSAR L band PolSAR datasets demonstrate the effectiveness and advantages of the proposed method in the quantitative characterization of scattering mechanisms, especially for highly oriented buildings.

Keywords: PolSAR; model-based polarimetric decomposition; rotated dihedral scattering model; cross-pol power; oriented buildings; branch condition

Citation: Duan, Y.; Quan, S.; Fan, H.; Xu, Z.; Xiao, S. A Five-Component Decomposition Method with General Rotated Dihedral Scattering Model and Cross-Pol Power Assignment. *Remote Sens.* **2023**, *15*, 4512. https://doi.org/10.3390/rs15184512

Academic Editor: Gerardo Di Martino

Received: 16 August 2023
Revised: 2 September 2023
Accepted: 11 September 2023
Published: 13 September 2023

1. Introduction

Polarimetric Synthetic Aperture Radar (PolSAR) can work day and night and is independent of weather conditions, becoming an important kind of sensor in the field of remoting sensing. By transmitting and receiving two orthogonal electromagnetic waves, PolSAR can acquire full polarization information of targets, which is widely used for disaster monitoring [1,2], urban areas extraction [3–5], ship detection [6,7], etc. Model-based polarimetric decomposition is a powerful tool to interpret the measured PolSAR data, which was pioneered by Freeman and Yamaguchi [8,9]. In the model-based decomposition, the measured polarimetric coherency matrix (or polarimetric covariance matrix) is divided into the weighted sum of several basic scattering models, such as surface (or odd-bounce), double-bounce, volume and helix scattering models. After obtaining the scattering powers of different components, the scattering mechanism of targets can be understood.

In the last two decades, researchers have carried out many explorations. Generally, all improved decomposition methods pursue good fitness between measured PolSAR data and established basic scattering models. They can be roughly divided into two categories. One is modifying or extending the basic scattering models to fit the measured PolSAR

data better. Considering different radar operating frequencies and complicated vegetation canopy scenes, many volume scattering models were proposed, in which the shapes of elementary scatters and the probability density functions of their orientation angles are taken into account [10–14]. The classic surface and double-bounce scattering models [15] are coherent and do not consider the cross-pol power induced by sloped terrains and oriented buildings. Therefore, incoherent surface and double-bounce scattering models were proposed to characterize their depolarization effects [16–18]. Additionally, many extended scattering models were introduced. In [19], Moriyama et al. presented the cross-scattering model for urban areas. The cross-scattering could be further classified as wire scattering or scattering from rotated dihedrals. In [20], Zhang et al. proposed a multiple-component decomposition method by introducing the wire scattering model. In [21], Hong et al. constructed the rotated diplane scattering model considering the cross-pol double-bounce component. From a similar point of view, Xiang et al. proposed the cross-scattering model for oriented urban areas [22]. In [23], considering the actual proportions of co-pol and cross-pol components for oriented buildings, Quan et al. modified Xiang's cross-scattering model using an eigenvalue-based descriptor and proposed the OOBs (Obliquely Oriented Buildings) scattering model. Based on compound scattering theory, Singh et al. further proposed compound dipoles, quarter-wave reflectors, oriented dipoles, oriented quarter-wave reflectors and mixed dipoles scattering models to physically interpret the off-diagonal elements of coherency matrix, namely, $\mathrm{Re}(T_{12})$, $\mathrm{Im}(T_{12})$, $\mathrm{Re}(T_{13})$, $\mathrm{Im}(T_{13})$ and $\mathrm{Re}(T_{23})$ [24].

Another category is transforming the measured PolSAR data to fit the existing basic scattering models. Polarimetric orientation angle compensation (OAC) or deorientation is the most commonly used manipulation, which rotates the coherency matrix about the radar line of sight (LOS) to minimize the cross-pol power, mitigating the overestimation of volume scattering (OVS) in oriented buildings to some extent [25–27]. From another point of view, researchers thought that the incorrect decomposition results might be caused by the inappropriate input coherency matrix, which was not reflection symmetric. Therefore, they dedicated to obtaining the reflection symmetric approximation of the coherency matrix and then performed the subsequent polarimetric decomposition [28,29]. Apart from the above-mentioned two categories of improvements in model-based polarimetric decomposition for PolSAR data, in recent years, researchers have been devoted to extending this excellent concept to the interpretation and application of dual-pol and hybrid-pol SAR data [30,31].

Although great advance has been achieved in model-based polarimetric decomposition, there still exists severe scattering mechanism ambiguity in highly oriented urban areas. Given this, we argue that both the refinement of the scattering model and the assignment of cross-pol power are indispensable. As a result, this paper simultaneously integrates these two aspects and thus proposes a five-component decomposition method to address the aforementioned problems.

This paper mainly consists of two parts. In the first part, the cross-scattering model for oriented urban areas is introduced, and then a general rotated dihedral scattering model is proposed. Based on this model, a five-component decomposition method is presented. Afterward, a simple branch condition with explicit physical meaning and an assignment strategy is established for model parameters inversion. In the second part, we demonstrate the proposed method on Radarsat−2 C band and UAVSAR L band PolSAR data and compare the decomposition results with other state-of-the-art methods qualitatively and quantitatively.

The novelties of the proposed method lie in the following three aspects: Firstly, we incorporate the general rotated dihedral scattering model to characterize the integral and internal cross-pol scattering from oriented buildings. This scattering model contributes to separating the cross-pol component of oriented buildings from the overall cross-pol power and then benefits the compensation of OVS in oriented urban areas. Secondly, we present a simple branch condition with explicit physical meaning. The experimental results demonstrate that this branch condition can accurately discriminate the dominant

scattering mechanism for different land covers. In addition, the proposed branch condition is roll-invariant. Finally, we design the cross-pol power assignment strategy to reasonably assign the cross-pol power between volume and rotated dihedral scattering. This strategy mitigates the underdetermined problem in the inversion process of model parameters, making the estimated parameters more accurate and improving the severe OVS in highly oriented buildings.

2. Methodology

2.1. General Rotated Dihedral Scattering Model for Oriented Urban Areas

The measured PolSAR data can be represented as a complex 2×2 backscattering matrix $\mathbf{S}$, which is shown as

$$\mathbf{S} = \begin{bmatrix} S_{HH} & S_{HV} \\ S_{VH} & S_{VV} \end{bmatrix} \tag{1}$$

where the subscripts H and V denote horizontal and vertical polarizations, respectively. The term S_{HV} indicates the scattering component when transmitting a vertical polarization signal and receiving a horizontal polarization signal, and other terms are defined similarly. According to the reciprocity theory, $S_{HV} = S_{VH}$ exists.

The target vector $\mathbf{k}_p$ based on the Pauli basis can be represented as

$$\mathbf{k}_p = \frac{1}{\sqrt{2}} \begin{bmatrix} S_{HH} + S_{VV} & S_{HH} - S_{VV} & 2S_{HV} \end{bmatrix}^T \tag{2}$$

where the superscript T denotes the transposition. The polarimetric coherency matrix $\mathbf{T}$ can be obtained from $\mathbf{k}_p$ by

$$\langle [\mathbf{T}] \rangle = \left\langle \mathbf{k}_p \mathbf{k}_p^{\dagger} \right\rangle = \begin{bmatrix} T_{11} & T_{12} & T_{13} \\ T_{12}^* & T_{22} & T_{23} \\ T_{13}^* & T_{23}^* & T_{33} \end{bmatrix} \tag{3}$$

where the superscript $*$ indicates complex conjugate and the superscript $\dagger$ represents conjugate transpose. The operation $\langle \cdot \rangle$ denotes ensemble average. Note that the diagonal and off-diagonal elements of $\mathbf{T}$ are real and complex numbers, respectively. Therefore, there are a total of nine degrees of freedom for the coherency matrix $\mathbf{T}$.

The conventional model-based decomposition methods consider the backscattering from urban areas to be mainly double-bounce scattering, which has proved to be practical only for buildings parallel to the radar flight path. For oriented buildings, the backscattered cross-pol signal may be more intense than the co-pol signal, resulting in a sharp decrease in double-bounce scattering power. Therefore, the double-bounce scattering model is not appropriate for describing the actual scattering from oriented urban areas. In addition, the forest area can also induce great cross-pol component, which can be characterized by the conventional volume scattering models. However, these volume scattering models are also inappropriate for describing the scattering behaviors of oriented buildings, which consist of many rotated dihedral structures. Therefore, there is a need to construct a separate scattering model that can characterize the integral and internal cross-pol scattering from oriented buildings well.

To start, we introduced several existing scattering models for oriented buildings. In [22], Xiang et al. proposed the cross-scattering model, which was modeled by ensemble averaging of scattering from rotated dihedrals. The coherency matrix of cross-scattering is expressed as

$$[\mathbf{T}]_{cross} = \begin{bmatrix} 0 & 0 & 0 \\ 0 & \frac{1}{2} - \frac{\cos(4\theta_{dom})}{30} & 0 \\ 0 & 0 & \frac{1}{2} + \frac{\cos(4\theta_{dom})}{30} \end{bmatrix} \tag{4}$$

where θ_{dom} is the estimated dominant orientation angle of buildings. It should be noted that only the T_{22} and T_{33} elements of cross-scattering matrix $[\mathbf{T}]_{cross}$ are not zero. When $\theta_{dom} = \pi/8$, the cross-scattering matrix (4) has the same form as the rotated diplane scattering model proposed in [21], which is shown as

$$[\mathbf{T}]_{rotated\_diplane} = \begin{bmatrix} 0 & 0 & 0 \\ 0 & 1/2 & 0 \\ 0 & 0 & 1/2 \end{bmatrix} \tag{5}$$

In [23], Quan et al. pointed out that when the orientation angle of dihedrals was not equal to zero, the backscattered cross-pol signal would be more intense than the co-pol signal. Therefore, the cross-scattering matrix shown in (4) was inconsistent with the actual situation, whose maximal difference between T_{22} and T_{33} elements was equal to $1/15$. From this point of view, they proposed the scattering model of OOBs as follows:

$$\begin{gathered} [\mathbf{T}]_{OOB} = \begin{bmatrix} 0 & 0 & 0 \\ 0 & O_{22} & 0 \\ 0 & 0 & O_{33} \end{bmatrix} \\ O_{22} = \frac{D_{OOB}}{D_{OOB} + \frac{D_{OOB}}{M - D_{OOB} + \xi}}, O_{33} = \frac{\frac{D_{OOB}}{M - D_{OOB} + \xi}}{D_{OOB} + \frac{D_{OOB}}{M - D_{OOB} + \xi}} \end{gathered} \tag{6}$$

where

$$D_{OOB} = \lambda_3 \frac{4\lambda_3}{SPAN} \left(1 - \frac{\lambda_1 - \lambda_2}{SPAN - 3\lambda_3}\right)^2 \tag{7}$$

D_{OOB} is an eigenvalue-based descriptor, which can represent the scattering characteristics of oriented buildings well. M is the maximal value of D_{OOB}. The design shown in (6) makes the inequality $O_{22} \ll O_{33}$ hold. It can be noticed that the scattering model of OOBs (6) has the same form as the cross-scattering model (4), except for the relative proportions between their T_{22} and T_{33} elements.

Given the priori guidance, in this paper, we introduce the general rotated dihedral scattering model (RDSM), which can be expressed as

$$[\mathbf{T}]_r = \begin{bmatrix} 0 & 0 & 0 \\ 0 & X_{22} & 0 \\ 0 & 0 & X_{33} \end{bmatrix} \tag{8}$$

where $X_{22} + X_{33} = 1$, $0 \leq X_{22}, X_{33} \leq 1$ and $X_{22} \leq X_{33}$. The restriction of $X_{22} \leq X_{33}$ is assumed considering the situation that cross-pol signal from rotated dihedrals is usually more intense than co-pol signal. The specific values of X_{22} and X_{33} are unknown, which are experimentally determined in the decomposition process.

Though researchers in [21–23] have devoted themselves to constructing refined scattering models for oriented buildings, there still exists severe OVS in these areas. This implies that only the refined scattering model for oriented buildings is not enough to mitigate scattering mechanism ambiguity.

2.2. Five-Component Decomposition with General Rotated Dihedral Scattering Model

Based on the general rotated dihedral scattering model (8), we propose a five-component decomposition method as follows:

$$\langle [\mathbf{T}] \rangle = f_s [\mathbf{T}]_s + f_d [\mathbf{T}]_d + f_v [\mathbf{T}]_v + f_h [\mathbf{T}]_h + f_r [\mathbf{T}]_r \tag{9}$$

where $\langle [\mathbf{T}] \rangle$ is the measured coherency matrix. $[\mathbf{T}]_s$, $[\mathbf{T}]_d$, $[\mathbf{T}]_v$, $[\mathbf{T}]_h$ and $[\mathbf{T}]_r$ are matrices of surface, double-bounce, volume, helix and rotated dihedral scattering, respectively. f_s, f_d,

f_v, f_h and f_r are corresponding expansion coefficients. The specific expressions of $[\mathbf{T}]_s$, $[\mathbf{T}]_d$, $[\mathbf{T}]_v$ and $[\mathbf{T}]_h$ are shown as

$$[\mathbf{T}]_s = \begin{bmatrix} 1 & \beta^* & 0 \\ \beta & |\beta|^2 & 0 \\ 0 & 0 & 0 \end{bmatrix}, [\mathbf{T}]_d = \begin{bmatrix} |\alpha|^2 & \alpha & 0 \\ \alpha^* & 1 & 0 \\ 0 & 0 & 0 \end{bmatrix} \tag{10}$$

$$[\mathbf{T}]_v = \frac{1}{4}\begin{bmatrix} 2 & 0 & 0 \\ 0 & 1 & 0 \\ 0 & 0 & 1 \end{bmatrix}, [\mathbf{T}]_h = \frac{1}{2}\begin{bmatrix} 0 & 0 & 0 \\ 0 & 1 & \pm j \\ 0 & \mp j & 1 \end{bmatrix} \tag{11}$$

According to (8)–(11), five equations can be obtained as

$$\begin{aligned} & f_s + f_d|\alpha|^2 + \tfrac{f_v}{2} = T_{11} \\ & f_s|\beta|^2 + f_d + \tfrac{f_v}{4} + \tfrac{f_h}{2} + f_r X_{22} = T_{22} \\ & f_s\beta^* + f_d\alpha = T_{12} \\ & \tfrac{f_v}{4} + \tfrac{f_h}{2} + f_r X_{33} = T_{33} \\ & \tfrac{f_h}{2} = |\mathrm{Im}(T_{23})| \end{aligned} \tag{12}$$

There are 8 unknown model parameters, including f_s, β, f_d, α, f_v, f_h, f_r and X_{22} (or X_{33}). Therefore, the inversion of model parameters shown in (12) is underdetermined. Assumptions should be made to fix two model parameters.

2.3. A Simple Branch Condition with Explicit Physical Meaning

In most model-based decomposition methods, the branch condition is used to discriminate the dominant scattering mechanism between surface and double-bounce scattering so as to fix the value of α or β. In [32], Maurya et al. investigated two widely used branch conditions. One is $\mathrm{Re}(S_{HH}S_{VV}^*)$ or $T_{11} - T_{22}$, another is $2T_{11} - SPAN + P_h$ or $T_{11}(\theta) - T_{22}(\theta) - T_{33}(\theta) + P_h$, where θ represents the polarimetric orientation angle. Through investigation, they found out that the mean alpha angle $\overline{\alpha}$ derived from eigenvalue–eigenvector decomposition showed superiority in discriminating against the dominant scattering mechanism. When $\overline{\alpha} \leq 45^\circ$ holds, surface scattering is dominant. Otherwise, if $\overline{\alpha} > 45^\circ$ holds, double-bounce scattering is dominant.

The average target vector $\mathbf{k}_0$ and corresponding coherency matrix $\mathbf{T}_0$ can be obtained by eigenvalue–eigenvector decomposition, which is shown in (13)

$$\begin{aligned} \mathbf{k}_0 &= \sqrt{\overline{\lambda}}e^{j\phi}\begin{bmatrix} \cos\overline{\alpha} & \sin\overline{\alpha}\cos\overline{\beta}e^{j\overline{\delta}} & \sin\overline{\alpha}\sin\overline{\beta}e^{j\overline{\gamma}} \end{bmatrix}^T \\ \mathbf{T}_0 &= \mathbf{k}_0\mathbf{k}_0{}^H \\ &= \overline{\lambda}\begin{bmatrix} \cos^2\overline{\alpha} & \cos\overline{\alpha}\sin\overline{\alpha}\cos\overline{\beta}e^{-j\overline{\delta}} & \cos\overline{\alpha}\sin\overline{\alpha}\sin\overline{\beta}e^{-j\overline{\gamma}} \\ \cos\overline{\alpha}\sin\overline{\alpha}\cos\overline{\beta}e^{j\overline{\delta}} & \sin^2\overline{\alpha}\cos^2\overline{\beta} & \sin^2\overline{\alpha}\cos\overline{\beta}\sin\overline{\beta}e^{j(\overline{\delta}-\overline{\gamma})} \\ \cos\overline{\alpha}\sin\overline{\alpha}\sin\overline{\beta}e^{j\overline{\gamma}} & \sin^2\overline{\alpha}\cos\overline{\beta}\sin\overline{\beta}e^{-j(\overline{\delta}-\overline{\gamma})} & \sin^2\overline{\alpha}\sin^2\overline{\beta} \end{bmatrix} \end{aligned} \tag{13}$$

From (13), it can be noted that $\frac{\cos^2\overline{\alpha}}{\sin^2\overline{\alpha}} = \frac{\mathbf{T}_0(1,1)}{\mathbf{T}_0(2,2)+\mathbf{T}_0(3,3)}$ [33], thus we can define k_0 as

$$k_0 = \frac{\cos^2\overline{\alpha}}{\sin^2\overline{\alpha}} = \frac{\mathbf{T}_0(1,1)}{\mathbf{T}_0(2,2) + \mathbf{T}_0(3,3)} \tag{14}$$

According to (14), the branch condition determined by $\overline{\alpha}$ is equivalent to that determined by k_0.

However, $\overline{\alpha}$ or k_0 is derived from eigenvalue–eigenvector decomposition, which is time-consuming for large-scale PolSAR data. To simplify the solution of the branch condition, we propose a simple branch condition with explicit physical meaning, which is similar to (14) and can be expressed as

$$k = \frac{T_{11}}{T_{22} + T_{33}} \tag{15}$$

Apparently, k can be directly obtained from the measured coherency matrix. When $k \geq 1$ holds, surface scattering is dominant. Otherwise, if $k < 1$ holds, double-bounce scattering is dominant. In addition, it can be noted that k is roll-invariant. Experiments on the Radarsat−2 C band and UAVSAR L band datasets show that the proposed branch condition k can discriminate the dominant scattering mechanism well (corresponding details can be found in Section 4.3). Consequently, we use (15) as the branch condition in this paper.

2.4. Assignment of Cross-Pol Power

In this subsection, an assignment strategy is designed to further solve the OVS and underdetermined problem. It can be noticed from (12) that the helix, volume, and cross-scattering models all contribute to cross-pol power (T_{33} term of coherency matrix). Among them, the expansion coefficient of helix scattering f_h can be determined directly by the imaginary part of T_{23}. Therefore, the following equation can be obtained:

$$\frac{f_v}{4} + f_{cro} X_{33} = T_{33} - \frac{f_h}{2} \tag{16}$$

From (16), it is noteworthy that if we know the relative proportion of cross-pol power between volume and rotated dihedral scattering, f_v can be determined straightforwardly. Thus, we define the relative proportion of cross-pol power from rotated dihedral scattering as f. By reformulating (16), f can be expressed as

$$f = \frac{f_r X_{33}}{T_{33} - \frac{f_h}{2}} \tag{17}$$

where $0 \leq f \leq 1$. In oriented urban areas, the cross-pol power is mainly caused by rotated dihedral scattering; thus, the value of f in this area should approximate to one. However, in vegetation areas such as forests, the cross-pol power is mainly induced by volume scattering from the canopy; therefore, the value of f should approximate to zero. If f can be appropriately determined in advance, the OVS that exists in [21–23] will be improved, and one more equation is added for model parameters inversion.

In this paper, the eigenvalue-based descriptor D_{OOB} shown in (7) is used to determine the value of f. This descriptor has been proven to highlight the polarimetric characteristics of OOBs effectively. More details about D_{OOB} can be found in [23]. To quantitatively describe the rotation degree of buildings, we define the rotation angle of buildings (α_{rot}) as that of the main street direction relative to the radar flight path, as illustrated in Figure 1. The range of α_{rot} is $(-45°, 45°]$, where the negative sign means clockwise rotation relative to the radar flight path. Generally, the larger the rotation angle, the larger the value of D_{OOB}. To determine f, some typically oriented buildings are chosen as training data in practical processing. In [34], Chen et al. concluded that the deorientation processing is invalid for oriented built-up patches whose dominant polarimetric orientation angles are greater than 22.5°. Therefore, considering the challenging situation for deorientation, we restrict the $|\alpha_{rot}|$ of training data to be greater than 22.5°. The value of f can be determined by D_{OOB} as

$$\begin{cases} f = 1, D_{OOB} \geq TH \\ f = \frac{D_{OOB}}{TH}, D_{OOB} < TH \end{cases} \tag{18}$$

where the threshold TH is determined as the minimum of calculated mean values of D_{OOB} from these selected typical areas. According to (18), the assignment of cross-pol power between vegetation and oriented buildings can be achieved by the incorporation of D_{OOB}.

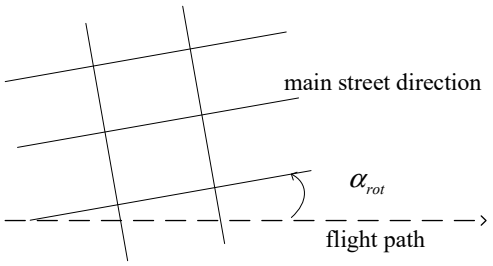

Figure 1. The definition of rotation angle of buildings.

2.5. Inversion of Model Parameters

From (12), we can directly obtain the value of f_h as

$$f_h = 2|\mathrm{Im}(T_{23})| \tag{19}$$

if $T_{33} - \frac{f_h}{2} < 0$ holds, then f_h is forced to be zero.

After deriving f from D_{OOB}, according to (16) and (17), we can obtain f_v and $f_r X_{33}$ as

$$\begin{aligned} f_v &= 4(1-f)(T_{33} - \tfrac{f_h}{2}) \\ f_r X_{33} &= f(T_{33} - \tfrac{f_h}{2}) \end{aligned} \tag{20}$$

Define $m = \frac{X_{22}}{X_{33}}$, then the range of m is $[0, 1]$ according to the restriction of $X_{22} \leq X_{33}$. Afterward, $f_r X_{22}$ and f_r can be derived as

$$\begin{aligned} f_r X_{22} &= m f_r X_{33} \\ f_r &= f_r X_{33} + f_r X_{22} = f_r X_{33}(1+m) \end{aligned} \tag{21}$$

Reorganize the remaining equations in (12) as

$$\begin{aligned} f_s + f_d|\alpha|^2 &= S \\ f_s|\beta|^2 + f_d &= D \\ f_s\beta^* + f_d\alpha &= C \end{aligned} \tag{22}$$

where

$$\begin{aligned} S &= T_{11} - \tfrac{f_v}{2} \\ D &= T_{22} - \tfrac{f_v}{4} - \tfrac{f_h}{2} - f_r X_{22} \\ &= T_{22} - \tfrac{f_v}{4} - \tfrac{f_h}{2} - m f_r X_{33} \\ C &= T_{12} \end{aligned} \tag{23}$$

By using the branch condition in (15), if $k \geq 1$ holds, surface scattering is dominant, and then α is set to be zero. From (22) and (23), f_s, β and f_d can be determined as follows:

$$f_s = S, \beta^* = \frac{C}{S}, f_d = D - \frac{|C|^2}{S} \tag{24}$$

If $k < 1$ holds, double-bounce scattering is dominant and then β is set to be zero. From (22) and (23), f_s, f_d and α can be derived as follows:

$$f_d = D, \alpha = \frac{C}{D}, f_s = S - \frac{|C|^2}{D} \tag{25}$$

Therefore, the scattering powers of these five components are

$$P_s = f_s(1 + |\beta|^2), P_d = f_d(1 + |\alpha|^2), P_h = f_h, P_r = f_r \tag{26}$$

$$P_v = SPAN - P_s - P_d - P_h - P_r \tag{27}$$

where $SPAN = T_{11} + T_{22} + T_{33}$ is the total scattering power.

However, the value of m is unknown. In this paper, we sample m in $[0, 1]$ at an interval of 0.1 and then calculate the corresponding decomposition results. Through analyzing the decomposition results corresponding to different values of m, we conclude that for areas such as non-oriented buildings, forests and oceans, the rotated dihedral scattering is insignificant (namely, f_r is relatively small) and thus m has a negligible impact on the decomposition results. In other words, the refinement of the rotated dihedral scattering model for these areas is insignificant, and we can make m be any value in $[0, 1]$. While for oriented urban areas in which rotated dihedral scattering is intense, all components are approximately constant with different values of m except for double-bounce and rotated dihedral scattering. Specifically, a larger m indicates a stronger rotated dihedral scattering as well as a weaker double-bounce scattering. The selection of optimal m should make the relative proportion between double-bounce and rotated dihedral scattering conform to the actual situation as much as possible. Unfortunately, it is very difficult to measure the actual relative proportion, and therefore the optimal m is unavailable. From a different perspective, we can choose a rational rather than optimal m to realize the inversion of model parameters. Considering the situation that the rotated dihedral scattering from oriented buildings is usually intense, m is set as 1 to obtain the strongest rotated dihedral scattering.

This manipulation seems to violate the generality of the general rotated dihedral scattering model in Equation (8), making it the same as the rotated diplane scattering model. However, it is noteworthy that they are derived from different perspectives. The rotated diplane scattering model is modeled by the ensemble averaging of scattering from randomly rotated dihedrals, while the general rotated dihedral scattering model is specified by maximizing the rotated dihedral scattering power according to the proposed assignment strategy. The latter is more acceptable since the derivation is realized based on actual distribution rather than empirical assumption. The details of choosing a rational m is given in the following section.

3. Experimental Results and Analysis

3.1. Data Description

In this section, spaceborne Radarsat−2 C band and airborne UAVSAR L band PolSAR datasets are used to conduct experiments. Figure 2a,b show the Pauli and optical images of Radarsat−2 data, respectively, which was acquired in San Francisco, USA, on 9 April 2008. The range and azimuth resolutions of the original single look complex (SLC) data are 4.7 m and 4.8 m, respectively, and the incidence angles in the near and far range are 28.02° and 29.82°, respectively. In the preprocessing stage, the number of azimuth looks is 2, and SimiTest filter [35] is used to suppress the speckle noise. The imaging scene consists of urban areas, oceans, forests, mountains, etc. Figure 2c,d illustrate the Pauli and optical images of UAVSAR data. The time of data acquisition is 9 November 2012, and the imaging location is San Diego, USA. The incidence angle ranges from 22° to 65° between near and far range. Similarly, multi-look processing and SimiTest filters are used to reduce the effect of speckle noise. The numbers of range and azimuth looks are 3 and 12, respectively. After multi-look processing, the range and azimuth resolutions are 5 m and 7 m, respectively. The land cover mainly consists of urban areas, some mountains, forests and oceans.

(**a**) (**b**) (**c**) (**d**)

Figure 2. (**a**) Pauli and (**b**) optical images of Radarsat−2 C band data. (**c**) Pauli and (**d**) optical images of UAVSAR L band data.

3.2. Decomposition Results for Radarsat−2 C Band Data

For Radarsat−2 C band data, four oriented urban areas (RB1-RB4, marked by red rectangles in Figure 2a) are chosen as training data. Their rotation angles are 42.2°, −42.6°, 34.5° and −27.3°, respectively. The mean values of D_{OOB} in these four areas are calculated as 0.0087, 0.0068, 0.0234 and 0.0088. Therefore, for Radarsat−2 C band data, the threshold TH to determine f is set as the minimal mean value of D_{OOB}, 0.0068. Afterward, the relative proportion of cross-pol power from rotated dihedral scattering, namely, the value of f, can be derived from (7) and (18). Figure 3 displays the image of f for Radarsat−2 data. It can be noted that the value of f is significant in oriented urban areas. In other areas, such as non-oriented urban areas, forests and oceans, the value of f is small. Therefore, it is expected that by incorporating f, the assignment of cross-pol power between volume and rotated dihedral scattering can be achieved.

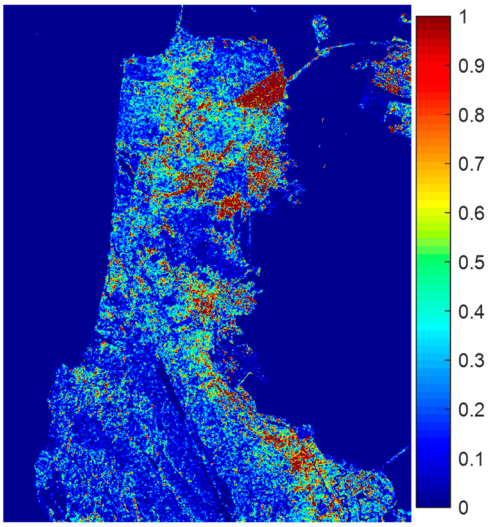

Figure 3. The image of f for Radarsat−2 data.

To quantitatively evaluate the decomposition results according to different values of m, here we choose four typical ROIs (ROI 1–ROI 4 are highly oriented buildings, slightly oriented buildings, forests and oceans, respectively, marked by black rectangles in Figure 2a) and compute the mean scattering power ratios (MSPRs) of five scattering components. Figure 4 shows the variations in the MSPRs of different scattering components with m in

these four selected ROIs. It is noted from Figure 4b–d that for slightly oriented buildings, forests and oceans, there is negligible impact of m on the MSPRs. This is because the assigned cross-pol power for rotated dihedral scattering in these areas by f is very small. Therefore, for areas in which rotated dihedral scattering is insignificant, there is no need to choose the optimal m, and any m in $[0, 1]$ is appropriate. However, from Figure 4a, it can be found that the MSPRs of double-bounce and rotated dihedral scattering change greatly with m in highly oriented buildings. As m increases, the MSPRs of double-bounce and rotated dihedral scattering become smaller and larger, respectively. Meanwhile, the impact of m on MSPRs of surface, volume and helix scattering can be ignored in this ROI. Considering the actual situation that the cross-pol signal backscattered from oriented buildings is more intense than co-pol signal, m is set as 1 to make the rotated dihedral scattering power larger in oriented urban areas.

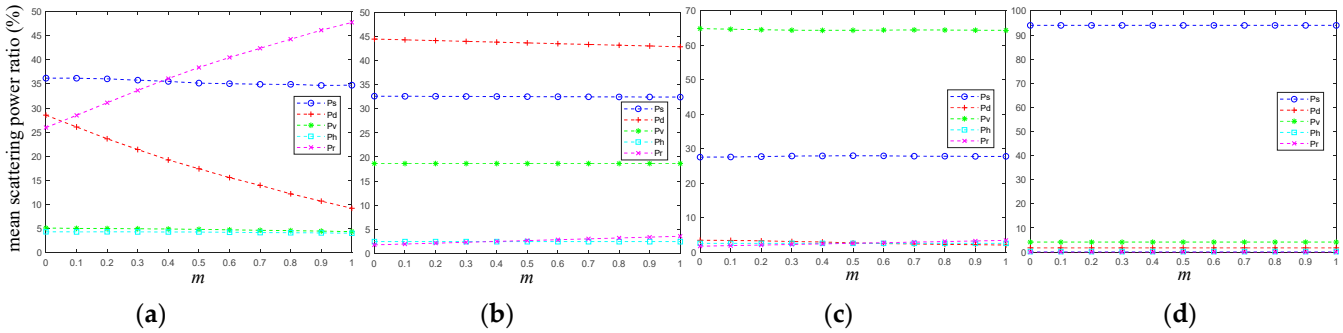

Figure 4. Mean scattering power ratios of different components according to m for Radarsat−2 data: (**a**) highly oriented buildings; (**b**) slightly oriented buildings; (**c**) forests; (**d**) oceans.

After determining the value of m, the decomposition results of the proposed method can be obtained. In this paper, H4D [21], X5D [22], Q5D [23], G5U [36] and W5D [37] are selected as comparison methods. Figure 5a–f display the pseudo-RGB images of the decomposition results by the proposed method and the other five comparison methods. The red, green and blue channels represent the building scattering (sum of all scattering components except volume and surface scattering), volume scattering and surface scattering, respectively. Note that the power redistribution rule is employed for W5D method as in [37].

Three oriented urban areas are selected (marked by the white rectangles in Figure 5a), and the corresponding zoomed optical and pseudo-RGB images are shown in Figure 6 for further comparison. Among them, Figure 6a1 presents a highly oriented urban area whose rotation angle is about 35°. It can be noted from Figure 6c1–g1 that all comparison methods suffer severe OVS, displaying green or yellow. The proposed method mitigates the scattering mechanism ambiguity in this area and shows red or magenta, as shown in Figure 6b1. The building arrangement illustrated in Figure 6a2 is relatively complicated. For the non-oriented or slightly oriented buildings, all methods can obtain correct decomposition results, showing magenta or orange. However, for highly oriented buildings, as shown in Figure 6a2 by the red rectangle, H4D, X5D and Q5D methods exhibit green, G5U and W5D methods display magenta or green, and the proposed method shows magenta. This demonstrates that the proposed method can obtain the most significant building scattering in highly oriented buildings. Figure 6a3 illustrates a coastal port area consisting of some oriented buildings and many neatly placed containers. For oriented containers (marked by the red rectangles in Figure 6a3), all comparison methods present green, while the proposed method shows magenta, illustrating that the proposed method performs better in this challenging area. In summary, from Figures 5 and 6, we can conclude that the proposed method demonstrates superiority in the characterization of building scattering, especially for highly oriented buildings.

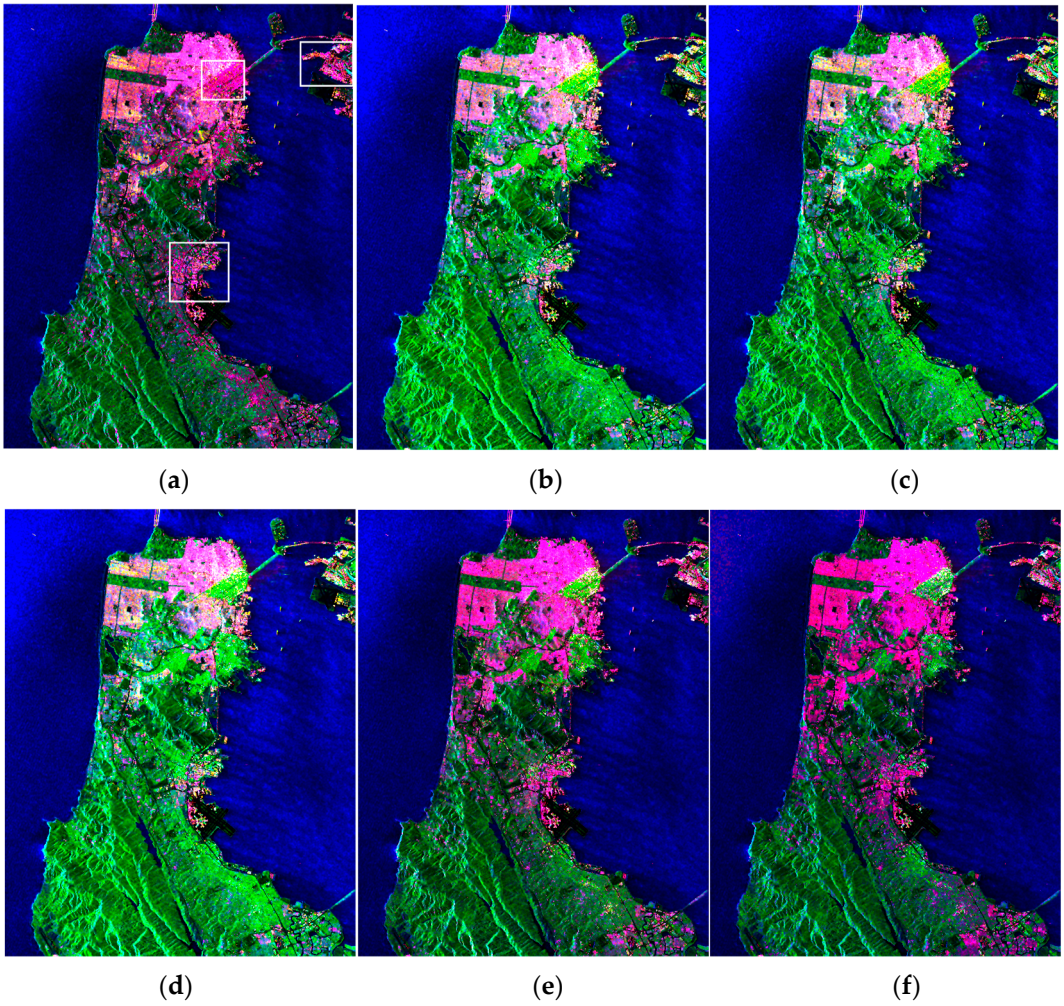

Figure 5. Decomposition results of Radarsat−2 data: (**a**) the proposed method; (**b**) H4D; (**c**) X5D; (**d**) Q5D; (**e**) G5U; (**f**) W5D (R: building scattering G: volume scattering B: surface scattering).

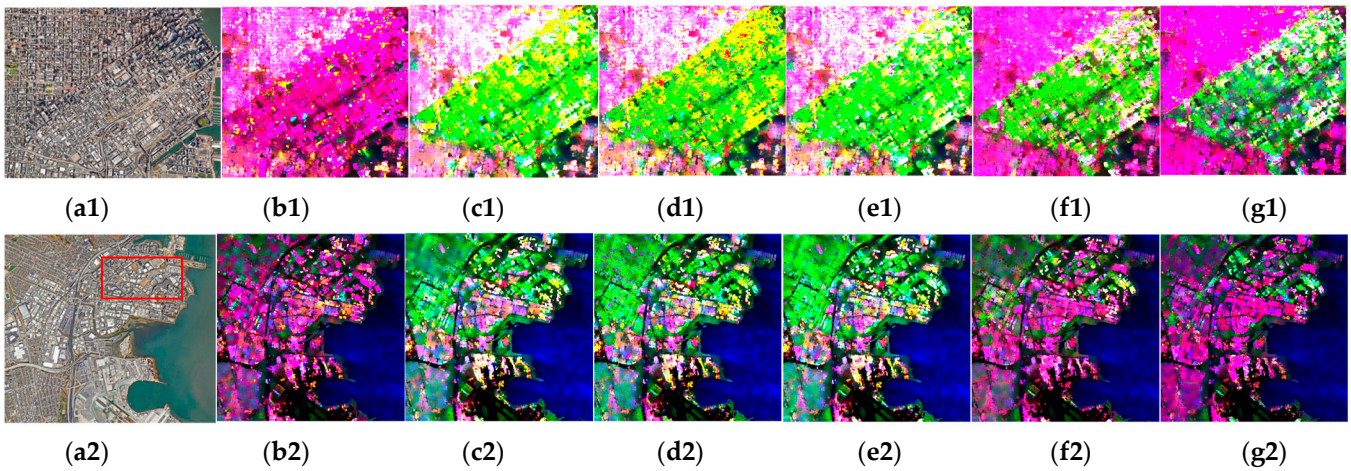

Figure 6. *Cont.*

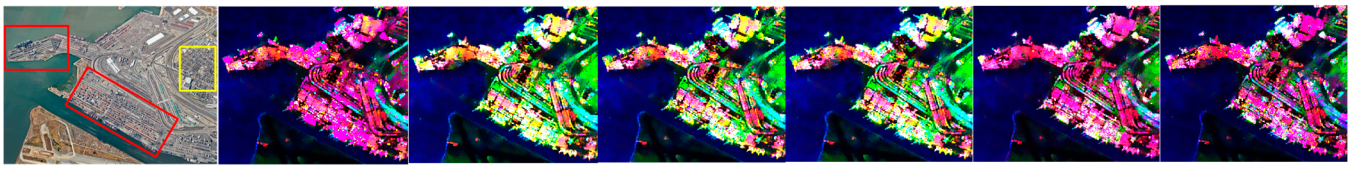

(**a3**) (**b3**) (**c3**) (**d3**) (**e3**) (**f3**) (**g3**)

Figure 6. Zoomed optical images and decomposition results of three oriented urban areas for Radarsat−2 data. (**a1**–**a3**) are optical images of the three oriented urban areas, respectively. (**b1**–**b3**), (**c1**–**c3**), (**d1**–**d3**), (**e1**–**e3**), (**f1**–**f3**) and (**g1**–**g3**) are pseudo-RGB images of the decomposition results by the proposed method, H4D, X5D, Q5D, G5U and W5D, respectively.

Figure 7a–e illustrate the power images of surface, double-bounce, volume, rotated dihedral and helix scattering by the proposed method. Figure 7c,d demonstrate that the proposed cross-pol power assignment strategy is effective, which greatly reduces the volume scattering power in oriented urban areas while retaining it in vegetation areas. Figure 7b,d indicate that the rotated dihedral scattering rather than double-bounce scattering is dominant for oriented urban areas.

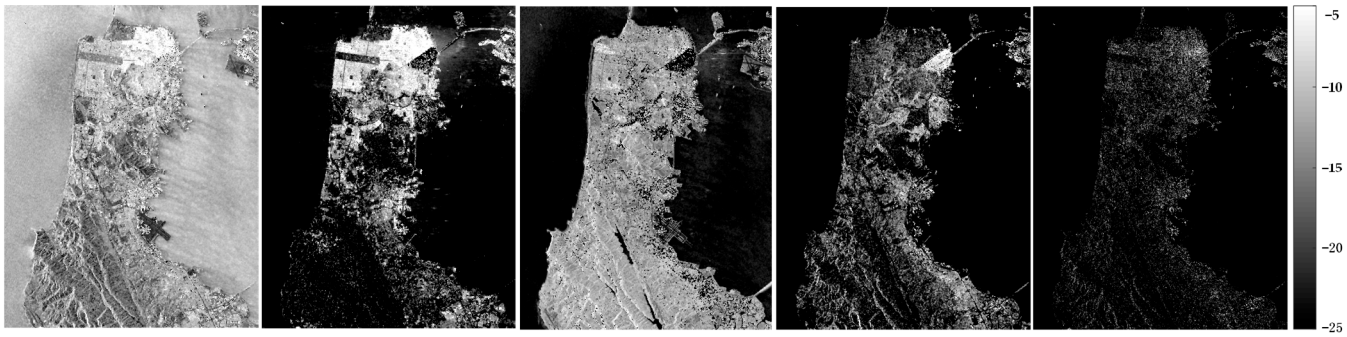

(**a**) (**b**) (**c**) (**d**) (**e**)

Figure 7. Power images of (**a**) surface, (**b**) double-bounce, (**c**) volume, (**d**) rotated dihedral and (**e**) helix scattering by the proposed method for Radarsat−2 data.

To quantitatively compare the decomposition results, we calculated the MSPRs of different scattering components by the proposed method and other comparison methods for the four chosen ROIs (marked by black rectangles in Figure 2a), as shown in Table 1. For ROI 1 (highly oriented buildings), the MSPRs of volume scattering are highest by H4D, X5D, Q5D, G5U and W5D approaches, which indicate severe OVS. However, in the proposed method, the MSPR of rotated dihedral scattering is the highest, followed by surface scattering, while the volume scattering is negligible. Therefore, the proposed method outperforms the other five methods in scattering interpretation for highly oriented urban areas. For ROI 2 (slightly oriented buildings), all the decomposition results show the highest MSPRs of double-bounce scattering, followed by surface scattering. Therefore, for slightly oriented urban areas, all methods can give correct interpretation results. For ROI 3 (forests), all methods obtain the highest MSPRs of volume scattering, followed by surface scattering. It is noteworthy that the MSPRs of volume scattering by G5U and W5D are much smaller than those of H4D, X5D, Q5D and the proposed method. For ROI 4 (oceans), all methods exhibit dominated surface scattering, and their performances are comparable.

Table 1. Mean scattering power ratios of different components (%) for Radarsat−2 data.

ROI	Method	Surface	Double-Bounce	Volume	Helix [1]	Rotated Dihedral [2]
ROI 1	H4D	5.85	19.35	**66.95**	\	7.85
	X5D	6.62	4.68	**64.82**	4.27	19.61
	Q5D	12.46	5.00	**67.32**	4.31	10.91
	G5U	9.60	23.32	**58.31**	4.61	4.16
	W5D	19.73	10.02	**45.06**	14.65	10.54
	Proposed	34.72	9.18	4.35	4.02	**47.73**
ROI 2	H4D	32.97	**41.65**	25.39	\	0.00
	X5D	32.56	**39.17**	25.80	2.46	0.01
	Q5D	33.22	**38.52**	25.80	2.46	4.76×10^{-3}
	G5U	36.29	**47.68**	11.63	2.03	2.37
	W5D	37.76	**44.80**	1.98	13.62	1.85
	Proposed	32.44	**42.87**	18.65	2.46	3.58
ROI 3	H4D	22.53	5.69	**70.56**	\	1.22
	X5D	26.79	1.75	**66.19**	2.45	2.82
	Q5D	26.18	1.75	**68.63**	2.51	0.94
	G5U	29.28	8.86	**53.02**	4.35	4.49
	W5D	29.46	4.91	**54.92**	3.76	6.95
	Proposed	27.77	2.01	**64.35**	2.50	3.37
ROI 4	H4D	**93.89**	1.73	4.38	\	0.00
	X5D	**94.01**	1.70	4.12	0.17	0.00
	Q5D	**94.01**	1.70	4.12	0.17	0.00
	G5U	**94.30**	2.16	2.74	0.45	0.35
	W5D	**94.07**	1.87	3.66	0.08	0.31
	Proposed	**94.01**	1.70	4.12	0.17	1.71×10^{-5}

[1] This component is oriented dipole scattering for G5U and double bounce-volume coupling scattering for W5D. [2] This component represents cross-pol double bounce scattering for H4D, cross-scattering for X5D, OOB scattering for Q5D, compound dipole scattering for G5U and surface–volume coupling scattering for W5D.

3.3. Decomposition Results for UAVSAR L Band Data

For UAVSAR L band data, four oriented urban areas are selected as training data to determine the threshold TH. These areas (RB1-RB4) are marked by red rectangles in Figure 2c, and their rotation angles are 43.7°, −43.2°, −28.6° and −42.6°, respectively. The mean values of D_{OOB} in these areas are 0.0048, 0.0071, 0.0055 and 0.0032. Therefore, the minimal mean value of D_{OOB}, namely, 0.0032, is set as the threshold TH. According to (7) and (18), the relative proportion of cross-pol power from rotated dihedral scattering can be determined in advance. The image of f is shown in Figure 8. It can be found that the value of f is significant in oriented urban areas. While for areas such as non-oriented buildings, mountains, forests and oceans, the values of f are much smaller.

In the last subsection, m is set as 1 for the proposed method. For UAVSAR data, we also test the variations in the decomposition results by the proposed method with m. For the four selected typical areas (ROI 1–ROI 4, which represent highly oriented buildings, non-oriented buildings, mountains and oceans, respectively, marked by yellow rectangles in Figure 2c), the MSPRs of different scattering components are calculated, as shown in Figure 9. It can be found from Figure 9b,d that the values of m have negligible impact on the decomposition results for non-oriented buildings and oceans. This is because the relative proportions of cross-pol power from rotated dihedral scattering in these areas are very small. From Figure 9c, for mountains, surface and volume scattering are dominant, which remain unchanged with m. Though the MSPRs of double-bounce and rotated dihedral scattering change slightly with m, none of them are dominant scattering components for mountains. Therefore, it can be assumed that the scattering powers for mountains are stable when changing m. Therefore, any m in $[0, 1]$ is suitable for areas in which rotated dihedral scattering is insignificant. From Figure 9a, for highly oriented buildings, the predetermined values of f are relatively large, resulting in the MSPRs of double-bounce

and rotated dihedral scattering changing greatly with m. The larger the value of m, the larger the MSPR of rotated dihedral scattering. Meanwhile, the MSPRs of the other three scattering components are approximately constant when changing m. Thus, m can be set as 1 to make the rotated dihedral scattering more intense for highly oriented buildings.

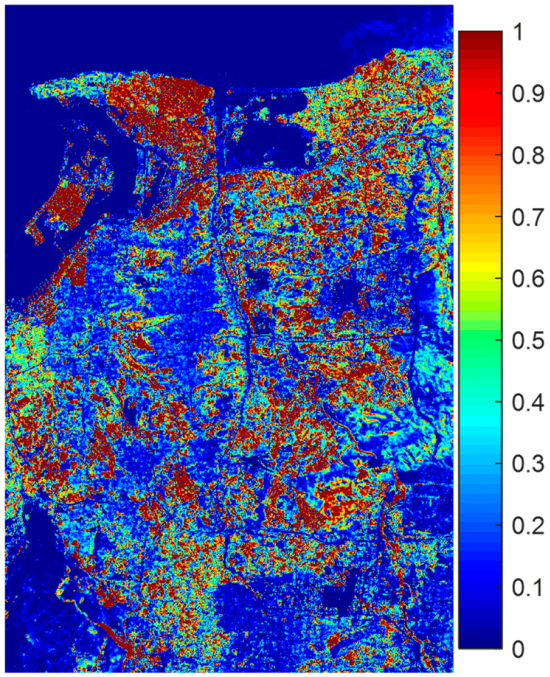

Figure 8. The image of f for UAVSAR data.

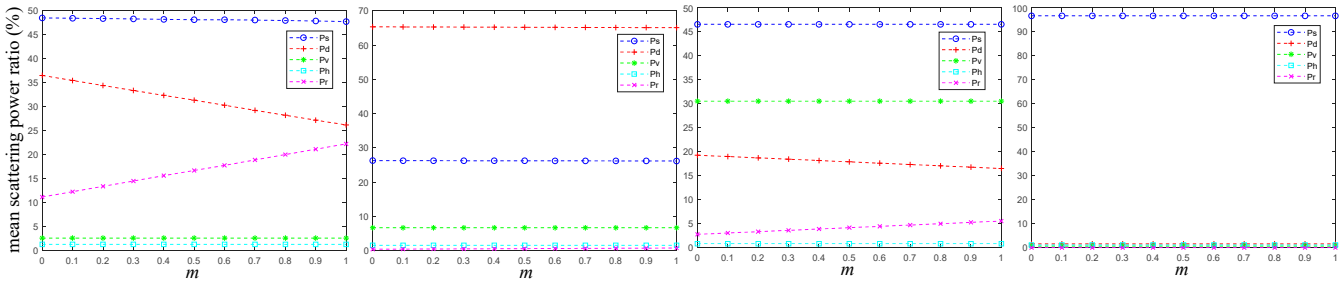

(**a**) (**b**) (**c**) (**d**)

Figure 9. Mean scattering power ratios of different components according to m for UAVSAR data: (**a**) highly oriented buildings; (**b**) non-oriented buildings; (**c**) mountains; (**d**) oceans.

By setting m as 1, the decomposition results of the proposed method can be obtained. The pseudo-RGB images, according to decomposition results by the proposed method, H4D, X5D, Q5D, G5U and W5D, are shown in Figure 10a–f, respectively. The red, green and blue channels of pseudo-RGB images represent building scattering, volume scattering and surface scattering, respectively. It can be noted that the proposed method shows superior performance, especially in oriented buildings, displaying magenta or purple in the top left part of Figure 10a. While the decomposition results of all comparison methods represent significant volume scattering in oriented urban areas, as shown in Figure 10b–f.

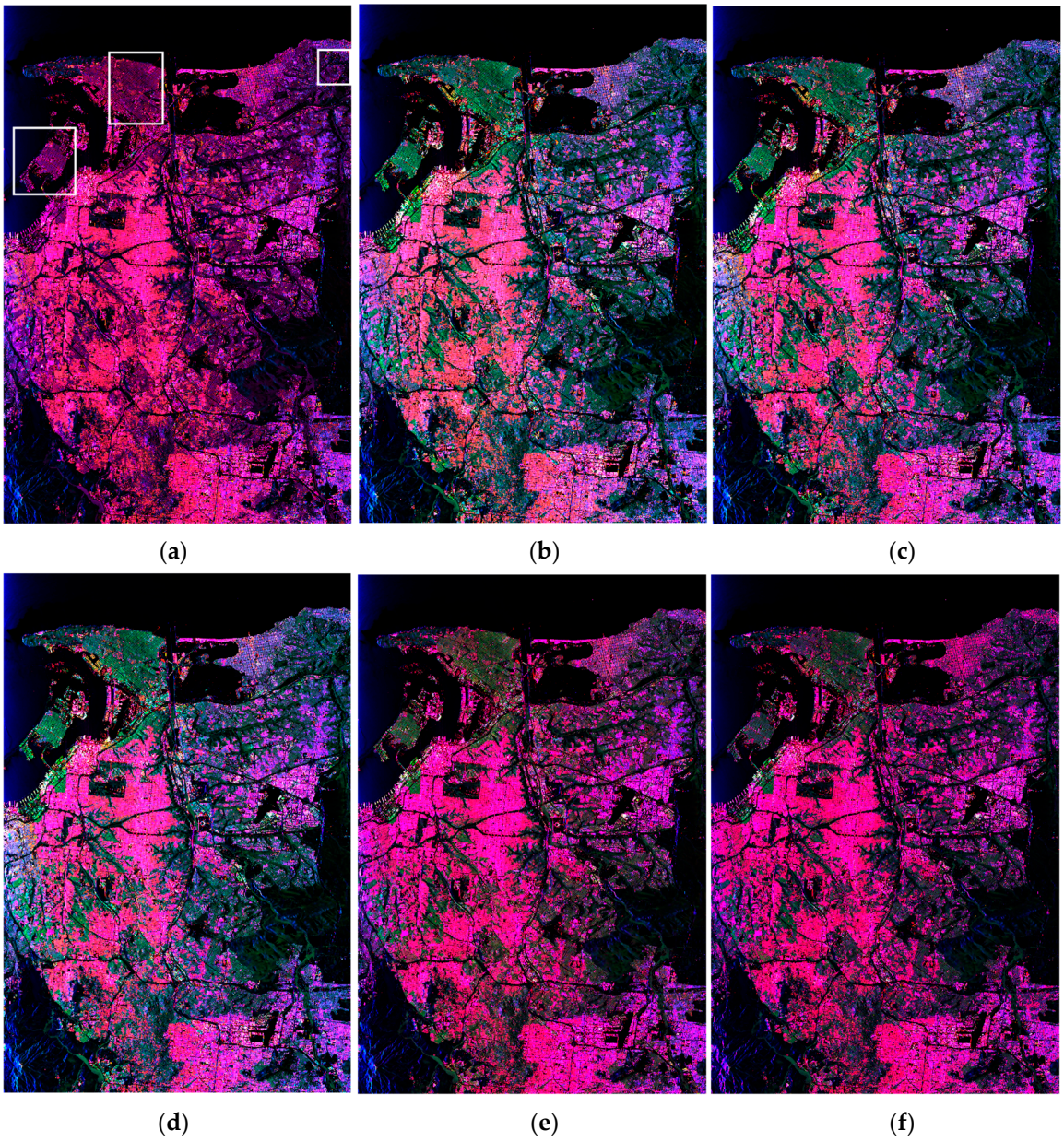

Figure 10. Decomposition results of UAVSAR data: (**a**) the proposed method; (**b**) H4D; (**c**) X5D; (**d**) Q5D; (**e**) G5U; (**f**) W5D (R: building scattering G: volume scattering B: surface scattering).

Figure 11 gives the zoomed optical images and decomposition results for the three chosen oriented urban areas (marked by a white rectangle in Figure 10a). Among them, Figure 11a1 presents an oriented urban area with a rotation angle of about $-29°$. It can be found from Figure 11b1–g1 that the proposed method shows dominated surface or building scattering in this area, while H4D, X5D, Q5D, G5U and W5D all suffer severe OVS. Figure 11a2 displays a highly oriented urban area with a rotation angle of about 44°. In this area, the proposed method still achieves superior scattering interpretation, while the other five comparison methods all fail to discriminate the oriented buildings from vegetation. Figure 11a3 illustrates a complicated urban area in which the arrangements of buildings are relatively diverse. It can be noticed that the proposed method performs well in this situation, reflecting intense building scattering for diversely oriented buildings. Meanwhile, the decomposition results of H4D, X5D and Q5D exhibit obvious scattering mechanism ambiguity. Though G5U and W5D can improve the OVS to some extent and display more purple or magenta than the other three comparison methods, there still exists

intense volume scattering in some oriented buildings. Therefore, we can conclude that the proposed method greatly mitigates the OVS in oriented urban areas and represents favorable scattering mechanism interpretation performance.

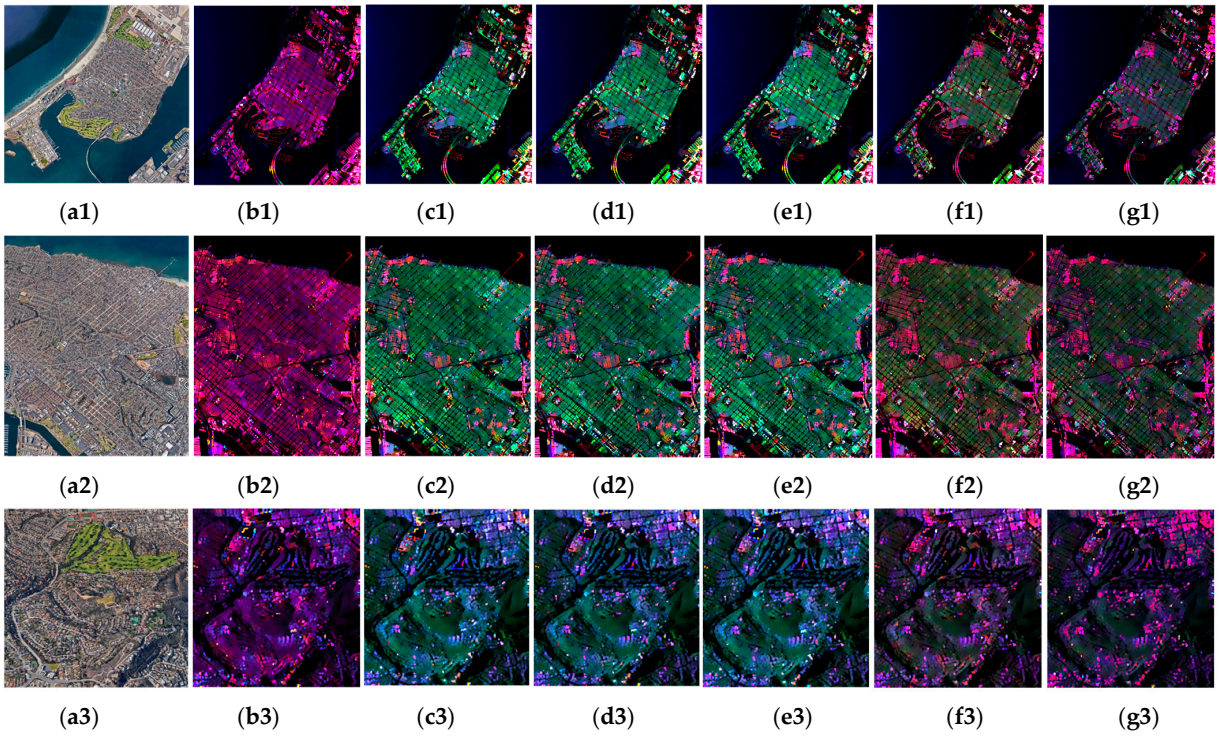

Figure 11. Zoomed optical images and decomposition results of three oriented urban areas for UAVSAR data: (**a1**–**a3**) are optical images of the three oriented urban areas, respectively. (**b1**–**b3**), (**c1**–**c3**), (**d1**–**d3**), (**e1**–**e3**), (**f1**–**f3**) and (**g1**–**g3**) are pseudo-RGB images of the decomposition results by the proposed method, H4D, X5D, Q5D, G5U and W5D, respectively.

Figure 12 shows the power images of surface, double-bounce, volume, rotated dihedral and helix scattering by the proposed method for UAVSAR data. It can be noticed from Figure 12c,d that the volume scattering of oriented urban areas is greatly reduced, and the rotated dihedral scattering in oriented buildings is more significant than in other areas such as mountains, non-oriented buildings and oceans. Therefore, the strategy of cross-pol power assignment effectively mitigates the scattering mechanism ambiguity in oriented urban areas.

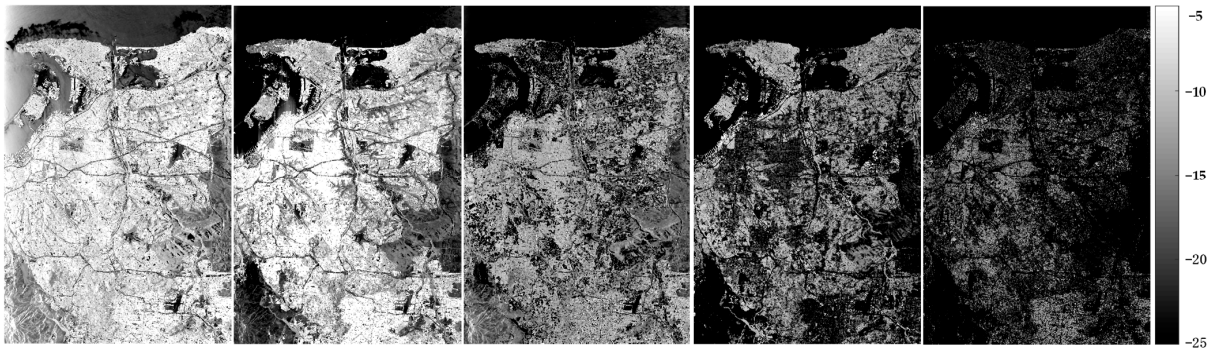

Figure 12. Power images of (**a**) surface, (**b**) double-bounce, (**c**) volume, (**d**) rotated dihedral and (**e**) helix scattering by the proposed method for UAVSAR data.

Table 2 gives the MSPRs of different scattering components in the four selected typical areas (ROI 1–ROI 4, marked by yellow rectangles in Figure 2c) for UAVSAR data. For ROI 1 (highly oriented buildings), H4D, X5D, Q5D and G5U present the highest MSPRs of volume scattering, followed by surface scattering. These indicate that severe OVS exists in the decomposition results of these four comparison methods. W5D obtains the highest MSPR of surface scattering, followed by those of double-bounce and volume scattering, which demonstrate that W5D can improve the OVS to some extent and correspondingly enhance building scattering. However, the proposed method achieves an insignificant value of 2.57% for volume scattering, largely due to the cross-pol power assignment strategy. Meanwhile, the surface, double-bounce and rotated dihedral scattering are greatly enhanced, improving the scattering mechanism ambiguity in highly oriented buildings. For ROI 2 (non-oriented buildings), all methods obtain comparative decomposition results. All of them give the highest MSPRs of double-bounce scattering, followed by surface scattering. For ROI 3 (mountains), H4D, X5D and Q5D obtain approximately equal MSPRs of volume and surface scattering. However, for G5U, W5D and the proposed method, the MSPRs of surface scattering are highest, followed by volume scattering. It can be noted that the MSPR of rotated dihedral scattering by the proposed method is 5.54%. This phenomenon may be caused by the rotated dihedral structures formed by tree trunks and ground surface, which exhibit similar backscattering to oriented buildings, and thus, less cross-pol power from volume scattering is assigned. For ROI 4 (oceans), all methods represent similar scattering interpretations, and the dominant scattering mechanism of oceans is surface scattering.

Table 2. Mean scattering power ratios of different components (%) for UAVSAR data.

ROI	Method	Surface	Double-Bounce	Volume	Helix [1]	Rotated Dihedral [2]
ROI 1	H4D	32.89	20.30	**46.81**	\	4.12×10^{-3}
	X5D	32.67	19.08	**46.83**	1.26	0.15
	Q5D	32.87	18.98	**46.78**	1.26	0.10
	G5U	29.90	29.46	**37.18**	1.88	1.59
	W5D	**35.55**	27.11	26.92	6.41	4.01
	Proposed	**47.75**	26.19	2.57	1.26	22.23
ROI 2	H4D	25.25	**63.84**	10.91	\	0.00
	X5D	26.65	**63.84**	8.03	1.48	0.00
	Q5D	27.20	**63.29**	8.03	1.48	0.00
	G5U	28.47	**65.93**	3.63	0.51	1.46
	W5D	28.20	**65.22**	2.58	1.98	2.01
	Proposed	26.13	**65.06**	6.63	1.48	0.70
ROI 3	H4D	41.20	16.04	**42.76**	\	0.00
	X5D	**41.64**	15.91	41.63	0.82	0.00
	Q5D	**41.64**	15.91	41.63	0.82	0.00
	G5U	**42.00**	19.79	34.75	1.42	2.04
	W5D	**44.75**	19.78	28.51	2.99	3.97
	Proposed	**46.58**	16.51	30.55	0.82	5.54
ROI 4	H4D	**95.66**	1.57	2.77	\	0.00
	X5D	**96.71**	1.58	0.64	1.07	0.00
	Q5D	**96.71**	1.58	0.64	1.07	0.00
	G5U	**96.15**	1.72	2.13	0.00	0.00
	W5D	**95.65**	1.57	2.78	0.00	0.00
	Proposed	**96.71**	1.58	0.64	1.07	1.06×10^{-6}

[1] This component is oriented dipole scattering for G5U and double bounce-volume coupling scattering for W5D.
[2] This component represents cross-pol double bounce scattering for H4D, cross-scattering for X5D, OOB scattering for Q5D, compound dipole scattering for G5U and surface–volume coupling scattering for W5D.

4. Discussion

4.1. The Importance and Feasibility of Cross-Pol Power Assignment

In this paper, an assignment strategy of cross-pol power is proposed, which determines the relative proportions of cross-pol power between volume and rotated dihedral scattering by the eigenvalue-based descriptor D_{OOB}. This strategy is crucial because in H4D, X5D and Q5D, though refined scattering models for oriented urban areas are presented, the inversion procedures of model parameters tend to assign more priority to an estimation of volume scattering, resulting in OVS in highly oriented buildings. Therefore, we use a cross-pol power assignment strategy to properly predetermine the contribution of volume scattering so as to estimate the contributions of other scattering components better.

In the stage of cross-pol power assignment, training data of typically oriented urban areas is necessary to determine the threshold TH. In this paper, we use two different PolSAR datasets and determine the corresponding thresholds (0.0068 for Radarsat−2 C band data and 0.0032 for UAVSAR L band data), which are confirmed to be effective for other Radarsat−2 C band datasets with similar incidence angles and other UAVSAR L band data with similar imaging scene. Therefore, the feasibility of the proposed method is acceptable.

It should also be noted that the exact optimal value of TH for different PolSAR images may be slightly inconsistent, even for those of the same sensor. As we all know, this is the most common case for all data-driven methods of threshold determination. Therefore, in future work, we will dedicate ourselves to proposing other techniques, such as the contrast enhancement of the D_{OOB} image for automatically obtaining the value of f and hence achieving the cross-pol power assignment without manual intervention.

4.2. The Importance of General Rotated Dihedral Scattering Model

In the proposed method, we also introduce the general rotated dihedral scattering model, whose specific form is experimentally determined the same as the rotated diplane scattering model in [21]. This general rotated dihedral scattering model is necessary because it describes the integral and internal cross-pol scattering from oriented buildings and provides the basis for the assignment strategy of cross-pol power.

4.3. The Validity of the Proposed Branch Condition

To demonstrate the validity of the proposed branch condition k, optical images and binary images obtained by k for Radarsat−2 and UAVSAR data are given in Figures 13 and 14, respectively. It can be found from Figures 13b and 14b that the oriented and non-oriented buildings marked by red ellipses represent dominated double-bounce scattering, while the marked forest and mountains show dominated surface scattering. In addition, the dominant scattering mechanism of oceans is surface scattering. Therefore, the proposed branch condition is effective in discriminating the dominant scattering mechanisms of typical land cover types.

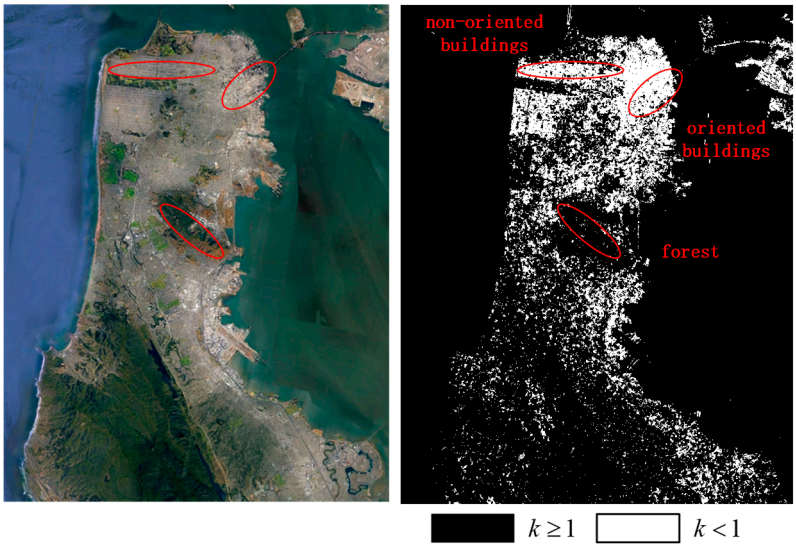

Figure 13. (**a**) Optical image and (**b**) binary image of k for Radarsat−2 data.

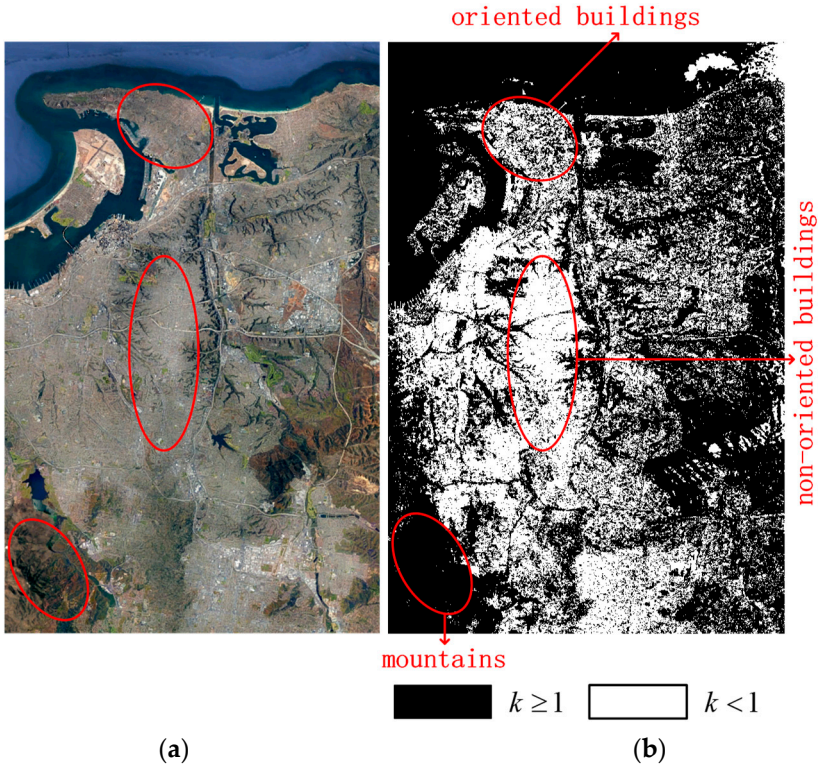

Figure 14. (**a**) Optical image and (**b**) binary image of k for UAVSAR data.

5. Conclusions

In this paper, we propose a five-component decomposition method with a general rotated dihedral scattering model and an assignment strategy of cross-pol power. Among them, the general rotated dihedral scattering model is established to properly characterize the integral and internal cross-pol scattering from oriented buildings, while the assignment strategy is designed to realize the assignment of cross-pol power between building and natural land cover scattering. Both these manipulations are applied to solve the intrinsic overestimation of volume scattering. Moreover, an alternative branch condition is proposed for the model parameters inversion, which makes the decomposition scheme more simple and physically clear. Experiments on the Radarsat−2 C band and UAVSAR L band PolSAR

datasets adequately demonstrate the effectiveness and superiority of the proposed method in scattering mechanism characterization, reflecting that the volume scattering is greatly reduced in oriented urban areas and thus mitigating the scattering mechanism ambiguity. Future works will focus on proposing other techniques to achieve the cross-pol power assignment without manual intervention and the applications of the proposed method in building extraction and other manmade target detection, etc.

Author Contributions: Y.D. is responsible for the design of the methodology, experimental data collection and processing, and preparation of the manuscript. S.Q. analyzed the data. H.F. and Z.X. helped analyze and discuss the results. S.X. is responsible for the technical support of the manuscript. All authors have read and agreed to the published version of the manuscript.

Funding: This research was funded by the National Natural Science Foundation of China under Grant 62001487.

Data Availability Statement: The Radarsat−2 data can be downloaded from https://ietr-lab.univ-rennes1.fr/polsarpro-bio/san-francisco/, accessed on 15 August 2023 and the UAVSAR data is available online https://search.asf.alaska.edu/, accessed on 15 August 2023.

Acknowledgments: The authors would like to thank MDA for the Radarsat−2 data and NASA/JPL for the UAVSAR data. They would also like to thank the editors and the anonymous reviewers for their meaningful comments.

Conflicts of Interest: The authors declare no conflict of interest. The funders had no role in the design of the study; in the collection, analyses, or interpretation of data; in the writing of the manuscript; or in the decision to publish the results.

References

1. Chen, S.; Sato, M. Tsunami Damage Investigation of Built-Up Areas Using Multitemporal Spaceborne Full Polarimetric SAR Images. *IEEE Trans. Geosci. Remote Sens.* **2012**, *51*, 1985–1997. [CrossRef]
2. Yamaguchi, Y. Disaster Monitoring by Fully Polarimetric SAR Data Acquired With ALOS-PALSAR. *Proc. IEEE* **2012**, *100*, 2851–2860. [CrossRef]
3. Fan, H.; Quan, S.; Dai, D.; Wang, X.; Xiao, S. Refined Model-Based and Feature-Driven Extraction of Buildings from PolSAR Images. *Remote Sens.* **2019**, *11*, 1379. [CrossRef]
4. Quan, S.; Zhang, T.; Wang, W.; Kuang, G.; Wang, X.; Zeng, B. Exploring Fine Polarimetric Decomposition Technique for Built-up Area Monitoring. *IEEE Trans. Geosci. Remote Sens.* **2023**, *61*, 5204719. [CrossRef]
5. Xiang, D.; Tang, T.; Hu, C.; Fan, Q.; Su, Y. Built-up Area Extraction from PolSAR Imagery with Model-Based Decomposition and Polarimetric Coherence. *Remote Sens.* **2016**, *8*, 685. [CrossRef]
6. Cui, X.C.; Tao, C.S.; Su, Y.; Chen, S.W. PolSAR Ship Detection Based on Polarimetric Correlation Pattern. *IEEE Geosci. Remote Sens. Lett.* **2021**, *18*, 471–475. [CrossRef]
7. Pan, X.; Wu, Z.; Yang, L.; Huang, Z. Ship Detection Method Based on Scattering Contribution for PolSAR Image. *IEEE Geosci. Remote Sens. Lett.* **2022**, *19*, 1–5. [CrossRef]
8. Freeman, A.; Durden, S.L. A Three-Component Scattering Model for Polarimetric SAR Data. *IEEE Trans. Geosci. Remote Sens.* **1998**, *36*, 963–973. [CrossRef]
9. Yamaguchi, Y.; Moriyama, T.; Ishido, M.; Yamada, H. Four-Component Scattering Model for Polarimetric SAR Image Decomposition. *IEEE Trans. Geosci. Remote Sens.* **2005**, *43*, 1699–1706. [CrossRef]
10. Arii, M.; Zyl, J.J.v.; Kim, Y. A General Characterization for Polarimetric Scattering from Vegetation Canopies. *IEEE Trans. Geosci. Remote Sens.* **2010**, *48*, 3349–3357. [CrossRef]
11. Antropov, O.; Rauste, Y.; Hame, T. Volume Scattering Modeling in PolSAR Decompositions: Study of ALOS PALSAR Data Over Boreal Forest. *IEEE Trans. Geosci. Remote Sens.* **2011**, *49*, 3838–3848. [CrossRef]
12. Sato, A.; Yamaguchi, Y.; Singh, G.; Park, S. Four-Component Scattering Power Decomposition with Extended Volume Scattering Model. *IEEE Geosci. Remote Sens. Lett.* **2012**, *9*, 166–170. [CrossRef]
13. Wang, Y.; Ainsworth, T.L.; Lee, J.S. Disk-Shaped Random Scatterers with Application to Model-Based PolSAR Decomposition. *IEEE Geosci. Remote Sens. Lett.* **2021**, *18*, 1961–1965. [CrossRef]
14. Wang, Z.; Zeng, Q.; Jiao, J. An Adaptive Decomposition Approach with Dipole Aggregation Model for Polarimetric SAR Data. *Remote Sens.* **2021**, *13*, 2583. [CrossRef]
15. Yamaguchi, Y.; Yajima, Y.; Yamada, H. A Four-Component Decomposition of PolSAR Images Based on the Coherency Matrix. *IEEE Geosci. Remote Sens. Lett.* **2006**, *3*, 292–296. [CrossRef]
16. Hajnsek, I.; Pottier, E.; Cloude, S.R. Inversion of Surface Parameters from Polarimetric SAR. *IEEE Trans. Geosci. Remote Sens.* **2003**, *41*, 727–744. [CrossRef]

17. Jiehong, C.; Zhang, H.; Wang, C. An Improved Four-Component Decomposition with Distributed Double-Bounce Scattering Model. In Proceedings of the 2012 International Conference on Computer Vision in Remote Sensing, Xiamen, China, 16–18 December 2012; pp. 344–349.
18. Lee, J.; Ainsworth, T.L.; Wang, Y. Generalized Polarimetric Model-Based Decompositions Using Incoherent Scattering Models. *IEEE Trans. Geosci. Remote Sens.* **2014**, *52*, 2474–2491. [CrossRef]
19. Moriyama, T.; Uratsuka, S.; Umehara, T.; Maeno, H.; Satake, M.; Nadai, A.; Nakamura, K. Polarimetric SAR Image Analysis Using Model Fit for Urban Structures. *IEICE Trans. Commun.* **2005**, *88*, 1234–1243. [CrossRef]
20. Zhang, L.; Zou, B.; Cai, H.; Zhang, Y. Multiple-Component Scattering Model for Polarimetric SAR Image Decomposition. *IEEE Geosci. Remote Sens. Lett.* **2008**, *5*, 603–607. [CrossRef]
21. Hong, S.; Wdowinski, S. Double-Bounce Component in Cross-Polarimetric SAR from a New Scattering Target Decomposition. *IEEE Trans. Geosci. Remote Sens.* **2014**, *52*, 3039–3051. [CrossRef]
22. Xiang, D.; Ban, Y.; Su, Y. Model-Based Decomposition with Cross Scattering for Polarimetric SAR Urban Areas. *IEEE Geosci. Remote Sens. Lett.* **2015**, *12*, 2496–2500. [CrossRef]
23. Quan, S.; Xiong, B.; Xiang, D.; Hu, C.; Kuang, G. Scattering Characterization of Obliquely Oriented Buildings from PolSAR Data Using Eigenvalue-Related Model. *Remote Sens.* **2019**, *11*, 581. [CrossRef]
24. Singh, G.; Mohanty, S.; Yamazaki, Y.; Yamaguchi, Y. Physical Scattering Interpretation of POLSAR Coherency Matrix by Using Compound Scattering Phenomenon. *IEEE Trans. Geosci. Remote Sens.* **2020**, *58*, 2541–2556. [CrossRef]
25. Lee, J.; Ainsworth, T.L.; Chen, K. The Effect of Orientation Angle Compensation on Polarimetric Target Decompositions. In Proceedings of the 2009 IEEE International Geoscience and Remote Sensing Symposium, Cape Town, South Africa, 12–17 July 2009; pp. IV-849–IV-852.
26. An, W.; Xie, C.; Yuan, X.; Cui, Y.; Yang, J. Four-Component Decomposition of Polarimetric SAR Images with Deorientation. *IEEE Geosci. Remote Sens. Lett.* **2011**, *8*, 1090–1094. [CrossRef]
27. Yamaguchi, Y.; Sato, A.; Boerner, W.; Sato, R.; Yamada, H. Four-Component Scattering Power Decomposition with Rotation of Coherency Matrix. *IEEE Trans. Geosci. Remote Sens.* **2011**, *49*, 2251–2258. [CrossRef]
28. Li, H.; Chen, J.; Li, Q.; Wu, G.; Chen, J. Mitigation of Reflection Symmetry Assumption and Negative Power Problems for the Model-Based Decomposition. *IEEE Trans. Geosci. Remote Sens.* **2016**, *54*, 7261–7271. [CrossRef]
29. An, W.; Lin, M. A Reflection Symmetry Approximation of Multilook Polarimetric SAR Data and Its Application to Freeman–Durden Decomposition. *IEEE Trans. Geosci. Remote Sens.* **2019**, *57*, 3649–3660. [CrossRef]
30. Kumar, A.; Das, A.; Panigrahi, R.K. Hybrid-Pol Based Three-Component Scattering Model for Analysis of RISAT Data. *IEEE J. Sel. Top. Appl. Earth Observ. Remote Sens.* **2017**, *10*, 5155–5162. [CrossRef]
31. Mascolo, L.; Cloude, S.R.; Lopez-Sanchez, J.M. Model-Based Decomposition of Dual-Pol SAR Data: Application to Sentinel-1. *IEEE Trans. Geosci. Remote Sens.* **2022**, *60*, 1–19. [CrossRef]
32. Maurya, H.; Panigrahi, R.K. Investigation of Branching Conditions in Model-Based Decomposition Methods. *IEEE Geosci. Remote Sens. Lett.* **2018**, *15*, 1224–1228. [CrossRef]
33. Cai, Y.; Zhang, X.; Jiang, J. Three-Component Decomposition for Polarimetric SAR Images Based on Coherency Matrix. In Proceedings of the PIERS Proceedings, Guangzhou, China, 25–28 August 2014.
34. Chen, S.W.; Ohki, M.; Shimada, M.; Sato, M. Deorientation Effect Investigation for Model-Based Decomposition Over Oriented Built-Up Areas. *IEEE Geosci. Remote Sens. Lett.* **2013**, *10*, 273–277. [CrossRef]
35. Chen, S.W.; Wang, X.S.; Sato, M. PolInSAR Complex Coherence Estimation Based on Covariance Matrix Similarity Test. *IEEE Trans. Geosci. Remote Sens.* **2012**, *50*, 4699–4710. [CrossRef]
36. Malik, R.; Singh, G.; Dikshit, O.; Yamaguchi, Y. General Five-Component Scattering Power Decomposition with Unitary Transformation (G5U) of Coherency Matrix. *Remote Sens.* **2023**, *15*, 1332. [CrossRef]
37. Wang, Y.; Yu, W.; Hou, W. Five-Component Decomposition Methods of Polarimetric SAR and Polarimetric SAR Interferometry Using Coupling Scattering Mechanisms. *IEEE J. Sel. Top. Appl. Earth Observ. Remote Sens.* **2021**, *14*, 6662–6676. [CrossRef]